

# Critical Point and Phase Behavior of the Pure Fluid and a Lennard-Jones Mixture

Jeffrey J. Potoff and Athanassios Z. Panagiotopoulos \*

*Institute for Physical Science and Technology and Department of Chemical Engineering,  
University of Maryland, College Park, MD 20742-2431*

(September 17, 1998)

## Abstract

Monte Carlo simulations in the grand canonical ensemble were used to obtain liquid-vapor coexistence curves and critical points of the pure fluid and a binary mixture of Lennard-Jones particles. Critical parameters were obtained from mixed-field finite-size scaling analysis and subcritical coexistence data from histogram reweighting methods. The critical parameters of the untruncated Lennard-Jones potential were obtained as  $T_c^* = 1.3120 \pm 0.0007$ ,  $\rho_c^* = 0.316 \pm 0.001$  and  $p_c^* = 0.1279 \pm 0.0006$ . Our results for the critical temperature and pressure are not in agreement with the recent study of Caillool (preprint, 1998) on a four-dimensional hypersphere. Mixture parameters were  $\epsilon_1 = 2\epsilon_2$  and  $\sigma_1 = \sigma_2$ , with Lorentz-Berthelot combining rules for the unlike-pair interactions. We determined the critical point at  $T^* = 1.0$  and pressure-composition diagrams at three temperatures. Our results have much smaller statistical uncertainties relative to comparable Gibbs ensemble simulations.

Typeset using REVTeX

---

\*To whom correspondence should be addressed. E-mail: thanos@ipst.umd.edu

## I. INTRODUCTION

Monte Carlo simulation is an effective tool for investigating equilibrium properties of fluids. Faster computers and improved algorithms such as the Gibbs ensemble [1–3] and extended ensembles [4–6] have greatly simplified the determination of phase coexistence properties for fluids with given intermolecular interactions. In Gibbs ensemble simulations, the usual approach to locating critical points is by fitting a power law to near-critical coexistence data. This procedure has limited accuracy and is unworkable for mixtures. In addition, finite-size effects near the critical point are often difficult to characterize and control [3,7–9], due to the variable extent of the two regions of Gibbs ensemble simulations.

Histogram reweighting methods [10–12] provide accurate data for the free energy of a system over a range of thermodynamic conditions from a small set of grand canonical Monte Carlo simulations. When combined with finite-size scaling (FSS) techniques [13,14] they can be used to obtain reliable estimates of critical parameters. These techniques had not, until recently, been applied to off-lattice systems. Wilding and Bruce showed how to extend these methods to continuous-space fluids by incorporating the concept of field mixing [15,16]. Mixed-field finite-size scaling analysis has been used to locate liquid-vapor critical points for a wide range of systems, including two-dimensional [17] and three-dimensional Lennard-Jones fluids [18] and chain molecules [19,20].

While mixed-field finite-size scaling theory has been used successfully for several pure fluids, little work has been done in the area of mixtures. Simulation studies of liquid-liquid critical phenomena for symmetric square well [21,22] and asymmetric polymer mixtures [23] have been performed. Studies of liquid-vapor critical phenomena have been limited to symmetric mixtures of Lennard-Jones particles [24].

The critical point of the pure Lennard-Jones fluid has been the subject of a number of theoretical and simulation studies. The location of the critical point depends on the method employed for the long range corrections. Wilding’s FSS study of the three-dimensional Lennard-Jones fluid [18] used a cutoff of  $2.5\sigma$  and resulted in  $T_c^* = 1.1876(3)$ ,  $\rho_c^* = 0.3197(4)$ ,

where the number in parenthesis refers to the uncertainty in the last digit. Results of Smit [25] for the full Lennard-Jones potential, using Gibbs ensemble Monte Carlo, were  $T_c^* = 1.316(6)$  and  $\rho_c^* = 0.304(6)$ . Caillol recently performed a FSS study for the full Lennard-Jones potential on the surface of a four-dimensional hypersphere [26]. His predictions of  $T_c^* = 1.326(2)$  and  $\rho_c^* = 0.316(2)$  differ from those of Smit by slightly more than the combined simulation uncertainties. In an attempt to rectify this discrepancy, we performed a FSS study for the full Lennard-Jones fluid under conventional periodic boundary conditions.

This paper is organized as follows. We begin with a brief section describing the histogram reweighting technique as it applies to binary mixtures. We follow this with an overview of mixed field finite size scaling theory. In Section IV, we present our results of simulations for the pure Lennard-Jones fluid and the mixture. A finite-size scaling analysis is performed, yielding critical points for both the pure fluid and the mixture. We discuss the differences in the effects of finite system size on the apparent critical point of the pure fluid and the mixture and between systems with the same potential, but different long-range corrections. Finally, we show how histogram reweighting can be used to generate highly accurate phase coexistence data over a wide range of thermodynamic conditions, while requiring only a small number of simulations.

## II. THEORETICAL BACKGROUND

In this section we provide a brief overview of the histogram reweighting and mixed-field finite-size scaling methods as they apply to a binary mixture. The methods can be easily generalized to mixtures of more than two components.

Simulations are performed in the grand canonical ensemble, in which the number of particles  $N_1$  and  $N_2$  fluctuate while the temperature  $T$  volume  $V$  and chemical potentials  $\mu_1, \mu_2$  are input parameters of the simulation. Over the course of the simulation, a histogram containing the number of particles of each species and the energy is collected. The probability of observing a configuration with a given number of particles  $N_1, N_2$  and configurational

energy  $E$  is:

$$P(N_1, N_2, E) = \Omega(N_1, N_2, V, E) \exp[\beta(\mu_1 N_1 + \mu_2 N_2 - E)] / \Xi(\mu_1, \mu_2, V, E), \quad (1)$$

where  $\Omega(N_1, N_2, V, E)$  is the microcanonical density of states.  $\Xi$  is the grand canonical partition function given by:

$$\Xi(\mu_1, \mu_2, V, E) = \sum_{N_1, N_2} \frac{1}{N_1! \Lambda_1^{3N_1}} \frac{1}{N_2! \Lambda_1^{3N_2}} \exp[\beta(\mu_1 N_1 + \mu_2 N_2)] \int d\vec{r}^{N_1+N_2} \exp[-\beta E(N_1 + N_2)] \quad (2)$$

Where  $\Lambda_i = \sqrt{h^2/2\pi m_i k_b T}$  is the de Broglie wavelength of particles of type  $i$ ,  $\beta = 1/k_b T$ , and  $E(N_1 + N_2)$  is the configurational energy of the system with coordinates  $\vec{r}^{N_1+N_2}$ .

In practice, it is impractical to work with 3-dimensional histograms as the range of phase space covered in a simulation can be quite large. Instead, it is more efficient to record periodically the set of  $N_1, N_2, E$  values. The required probability distribution is extracted from this list at the end of the simulation.

In general, it is not possible to cover all thermodynamic states of interest from a single simulation. Instead, multiple simulations are required at various chemical potentials and temperatures. The histograms which result from the simulations are combined according to the method outlined by Ferrenberg and Swendsen [11,12] to form a unified distribution which can be reweighted to the conditions of interest. The distribution formed by combining  $R$  histograms is given by:

$$P_{\mu_1, \mu_2, \beta}(N_1, N_2, E) = \frac{\sum_{n=1}^R P_n(N_1, N_2, E) \exp[\beta(\mu_1 N_1 + \mu_2 N_2 - E)]}{\sum_{m=1}^R K_m \exp[\beta_m(\mu_{1m} N_1 + \mu_{2m} N_2 - E - f_m)]} \quad (3)$$

where

$$\exp[f_n] = \sum_{N_1, N_2, E} P(N_1, N_2, E) \quad (4)$$

$K_m$  is the total number of observations for the run  $m$ . The values of  $f_n$  are found self-consistently by iterating 3 and 4.

In order to combine multiple histograms, a reasonable amount of overlap must be present between neighboring histograms. When determining phase coexistence properties, there must be a connection between the liquid and vapor at the conditions of interest. In most cases it is convenient to bridge the liquid and vapor regions with a run near the critical point. Additional histograms are added on the liquid and vapor sides as one progresses along the coexistence curve. This avoids the problem of the formation of interfaces and the need to cross over the free energy barrier which grows as one moves away from the critical point. An alternative method is to overcome the large free energy barrier separating liquid from vapor at low temperatures through the application of the multicanonical method of Berg and Neuhaus [27].

The pressure of the system is related to the area under the 3-dimensional probability distribution by:

$$\beta p = \frac{\ln \Xi(\mu_1, \mu_2, V, E)}{V} + \text{constant} = \ln \sum_{N_1, N_2, E} \Omega(N_1, N_2, V, E) \exp[\beta(\mu N_1 + \mu N_2 - E)] \quad (5)$$

The area under the probability distribution gives a reliable estimate of the partition function, which is required to determine the additive constant in equation 5. To determine this constant, the partition function is calculated at low densities. A plot of  $\ln \Xi$  vs.  $N$  gives a straight line of unit slope, which shows the system behaves as an idea gas at these conditions. It is possible to extrapolate  $\ln \Xi$  to the  $N = 0$  limit, with the y intercept representing the additive constant.

Near phase coexistence a bimodal distribution of densities is expected. Phase coexistence is determined by adjusting the chemical potentials of the two components until equal area is found under the two peaks. Coexistence densities and mole fractions are calculated by taking the weighted average under each peak.

The principle of critical point universality requires that the critical behavior of fluid mixtures be in the same universality class as that of pure fluids and the Ising model [28]. For pure fluids, the critical behavior of the ordering operator distribution assumes a scaling form that matches the universal order parameter distribution appropriate for the 3-dimensional

Ising model [16–18]. Therefore, the ordering operator distribution for the binary mixture must also assume a scaling form that matches the universal fixed point ordering operator distribution  $\tilde{p}_m^*(x)$ . By analogy to the pure fluid, the ordering field for a binary mixture may be written as a linear combination of the temperature and chemical potential differences of each component:

$$h = \mu_1 - \mu_{1c} - s_1(T_c - T) - s_2(\mu_2 - \mu_{2c}) \quad (6)$$

where  $s_1$  and  $s_2$  are system specific parameters that control the degree of field mixing. This is a slightly different formulation than the work of Anisimov *et al* who derived the scaling fields for a binary mixture as a linear combination of  $\Delta T = T - T_c$ ,  $\Delta\mu_1 = \mu_1 - \mu_{1c}$  and  $\Delta\mu = \mu - \mu_c$ , where  $\mu = \mu_2 - \mu_1$  [29]. For a pure fluid, the proper ordering field is obtained by taking  $s_2 = 0$ . The critical point is found by tuning the chemical potentials  $\mu_1, \mu_2$  and the field mixing parameters  $s_1, s_2$  at a fixed temperature such that  $P(N_1, N_2, E)$  collapses onto  $\tilde{p}_m^*(x)$ .

The matching condition, however, does not imply the possibility of directly measuring the critical parameters. As we shall see, a finite-size shift occurs in the apparent critical parameters as a result of field mixing. From [19] we see that the density  $\rho$  is given by:

$$\rho = \mathcal{M} - s\mathcal{E} \quad (7)$$

Where  $\mathcal{E}$  and  $\mathcal{M}$  are the energy and ordering operator, respectively. For models with Ising symmetry,  $\mathcal{M}$  is the magnetization, while  $\mathcal{E}$  is the energy density. At the critical point, the critical density can be written as:

$$\langle \rho \rangle_c = \langle \mathcal{M} \rangle_c - s \langle \mathcal{E} \rangle_c \quad (8)$$

Since  $P(\mathcal{M})$  is symmetric, the value of  $\langle \mathcal{M} \rangle_c$  is independent of system size. The energy distribution  $P(\mathcal{E})$ , however, is not symmetric. As a result,  $\langle \mathcal{E} \rangle_c$  is expected to vary with system size like:

$$\langle \mathcal{E} \rangle_c(L) - \langle \mathcal{E} \rangle_c(\infty) \sim L^{-(d-1/\nu)} \quad (9)$$

Combining equations 8 and 9, we expect  $\langle \rho \rangle_c$  to vary with system size as the energy operator:

$$\langle \rho \rangle_c (L) - \langle \rho \rangle_c (\infty) \sim L^{-(d-1/\nu)} \quad (10)$$

For a mixture, we see similar scaling behavior for the critical mole fraction [23]:

$$\langle x \rangle_{1c} (L) - \langle x \rangle_{1c} (\infty) \sim L^{-(d-1/\nu)} \quad (11)$$

The finite-size scaling behavior of the critical pressure follows a similar behavior. The finite-size shift of the  $P(N_1, N_2, E)$  distribution comes from field mixing. This field mixing will manifest itself through a finite-size shift in the energy operator only, since the magnetization is symmetric and  $\langle \mathcal{M} \rangle_c$  is independent of system size. The pressure,  $p$ , is proportional to the area under the  $P(N_1, N_2, E)$  distribution, hence we submit:

$$\langle p \rangle_c (L) - \langle p \rangle_c (\infty) \sim \langle \mathcal{E} \rangle_c (L) - \langle \mathcal{E} \rangle_c (\infty) \sim L^{-(d-1/\nu)} \quad (12)$$

as the relationship for the finite-size scaling of the critical pressure.

### III. MONTE CARLO SIMULATIONS

In this work, we study systems of particles interacting via the Lennard-Jones potential:

$$U(r_{ij}) = 4\epsilon_{ij} \left[ \left( \frac{\sigma_{ij}}{r_{ij}} \right)^{12} - \left( \frac{\sigma_{ij}}{r_{ij}} \right)^6 \right] \quad (13)$$

where  $U$  is the configurational energy of pair interaction,  $r_{ij}$  is the distance between particles  $i$  and  $j$  and  $\epsilon_{ij}$ ,  $\sigma_{ij}$  are potential parameters for the  $ij$  interaction. The Lorentz-Bethelot combining rules were used to calculate the cross potential parameters for the mixture. The potential parameters of component 1 were used to obtain reduced quantities in the standard way, namely for the temperature  $T^* = k_B T / \epsilon_{11}$ , the density  $\rho^* = N \sigma_{11}^3 / V$  and the pressure  $p^* = p \sigma_{11}^3 / \epsilon_{11}$

Truncation of the potential has an important effect on the phase behavior and the critical properties [25]. In the present study, we are interested in obtaining the properties of the

full (untruncated) potential. Long-range corrections were applied in every simulation step, since the density of the system fluctuates. Corrections were performed with the method of Theodorou and Suter [30]. In this approach, all interactions between molecules in the simulation cell and their minimum image neighbors are included. The long-range correction is calculated by integrating the potential in two parts, the first from  $L/2$  to  $\sqrt{3}/2L$  using the corrected radial distribution function given by equation(13) in [30]. The second part is calculated by assuming  $g(r) = 1$  and integrating from  $\sqrt{3}/2L$  to  $\infty$ . The advantage of the Theodorou-Suter method is that corrections to the energy are significantly smaller than corrections using the "standard" cutoff of  $L/2$ .

The first system studied was the pure Lennard-Jones fluid. Short exploratory runs with  $V = 125$  were used to obtain initial estimates of the critical temperature. This was followed by simulations for  $V = 216, 343, 512, 729, 1000, 1728$  and  $2744$  near the apparent  $T_c^*$ . Runs of 200 million Monte Carlo Steps (MCS) were used for  $V = 216, 343$  and  $512$ . Runs of up to 1 billion MCS were required to gather accurate statistics for the larger system sizes. The simulation data were stored in the form of a list containing  $N$  and  $E$  for a given configuration with samples being taken every 500 MCS. Due to the high computational cost,  $V = 2744$  data were collected only near the critical point. As a result, they can be used to obtain  $T_c^*$  and  $\rho_c^*$ , but not  $p_c^*$ .

The binary mixture studied had  $\sigma_1 = \sigma_2 = 1.0$  and  $\epsilon_1 = 1.0, \epsilon_2 = 0.5$ . These values were chosen to allow for direct comparison between our results and those of Harismiadis *et al* [31]. Since finite-size effects are small away from the critical point, we used the smallest possible volume for sub-critical runs that would yield reliable results, which in this case was  $V = 216$ . Histograms collected near the critical point were reweighted to lower pressures to determine where additional simulations were required. When the coexistence density distributions became sufficiently noisy so that coexistence properties could not be reliably calculated, additional simulations were performed near the predicted coexistence chemical potentials. In this way, we were able to step around the liquid-vapor coexistence curve with a minimal amount of guessing. A total of seven simulations, covering a range of solvent

mole fractions from  $x_1 = 0.0$  to  $x_1 = 1.0$  at the relevant liquid and vapor densities, were performed at  $T^* = 1.0$ .

Each simulation was 20 million MCS in length with an equilibration period of 1 million MCS. Phase coexistence data were calculated for  $T^* = 0.9, 1.0$  and  $1.1$  by reweighting the simulation data collected at  $T^* = 1.0$ . To determine the effects of system size on the location of the critical point, simulations were performed for a range of volumes,  $V = 216, 343, 512, 1000$  and  $1728$ , at  $T^* = 1.0$ . For  $V = 216, 343$  and  $512$  runs of 200 million MCS were used, while for the largest two systems up to 500 million MCS were required. The simulation data for all runs were stored in the form of a list containing  $N_1, N_2$  and  $E$  for a given configuration with samples being taken every 1000 MCS. The necessary probability distributions were constructed from these lists upon completion of the simulation.

For the  $V = 216$  system, simulations performed in the liquid phase required approximately 1 CPU hour per 20 million MCS on a 500MHz DEC Alpha processor. Vapor phase simulations were much shorter, since the average number of particles was lower. Total CPU time required to determine the complete coexistence curves for  $T^* = 0.90 - 1.10$  was approximately 5 CPU hours.

Statistical uncertainties for both the mixture and the pure fluid were calculated by performing 3 independent sets of simulations with different random number seeds. The standard deviation of the results from the three simulation sets was used as the statistical uncertainty estimate.

## IV. RESULTS AND DISCUSSION

### A. Pure Fluid

The location of the critical point for the pure Lennard-Jones fluid has been the subject of numerous studies. It has been shown that truncation of the potential has a considerable effect on the location of the critical point [8,25].

For the potential truncated at  $2.5\sigma$ , Gibbs ensemble simulations, in which finite-size effects were carefully studied, yielded  $T_c^* = 1.176(8)$  and  $\rho_c^* = 0.33(1)$  [8]. These agree reasonably well with the results of Wilding's finite-size scaling study,  $T_c^* = 1.1876(3)$ ,  $\rho_c^* = 0.3197(4)$  [18].

Most current estimates of the critical point of the untruncated Lennard-Jones fluid are based on Gibbs ensemble simulations of subcritical behavior and extrapolation to the critical point by using the scaling laws for the width of the coexistence curve. Smit reports  $T_c^* = 1.316(6)$ ,  $\rho_c^* = 0.304(6)$  [25]. Lotfi, using the  $NpT$  plus test particle method, predicted  $T_c^* = 1.31$  and  $\rho_c^* = 0.314$  [32].

The only other finite-size scaling study of the full Lennard-Jones pure fluid is the recent work of Caillol [26], who simulated the full Lennard-Jones potential on the surface of a four-dimensional hypersphere, a technique that does not require long-range corrections. In the present study, conventional periodic boundary conditions with long-range corrections are used, so it is of interest to compare the two sets of critical parameter estimates and the magnitude of finite-size effects. Our pure fluid results also provide a baseline for comparisons of the finite-size effects between the pure fluid and the mixture.

Figure 1 shows the ordering operator distributions at the critical point for the pure fluid and mixture. System size is  $V=216$  for both cases. Our data match the universal distribution for the Ising 3-dimensional universality class quite well.

Finite-size scaling of the apparent critical temperature  $T_c^*(L)$  is given by [18]:

$$T_c^*(\infty) - T_c^*(L) \sim L^{-(\theta+1)/\nu} \quad (14)$$

In Figure 2 we plot the apparent critical temperature,  $T_c^*(L)$  as a function of  $L^{-(\theta+1)/\nu}$ , where  $L$  is the length of the simulation cell, with  $\theta = 0.54$  and  $\nu = 0.629$  [14,33]. The error bars are directly related to the simulation run length. Very long runs were used for the larger ( $V > 512$ ) system sizes, resulting in reduced error bars when compared to the smaller systems. Extrapolating to  $L = \infty$  we calculated  $T_c^* = 1.3120(7)$ , which is near the value of 1.316(6) reported by Smit [25]. Our new estimate, however, has a significantly smaller statistical

uncertainty. The extrapolated infinite-system value for the critical chemical potential from our runs was  $\mu_c^* = -3.562(1)$ , or  $\beta_c \mu_c = -2.715(1)$ .

In Figure 3 we plot the critical density vs.  $L^{-(d-1/\nu)}$ . This quantity  $\rho_c^*(L)$  varies relatively little with system size, differences being near the statistical uncertainties of the data. Linear regression of the data to  $L = \infty$  yields  $\rho_c^*(\infty) = 0.316(1)$ . This value differs significantly from the Smit calculation of  $\rho_c^* = 0.304(6)$ . A possible source for the discrepancy has been given by Valleau who found that significant shifts in the coexistence curve can occur in Gibbs ensemble simulations near the critical point if the difference between the number of particles in the two simulation cells is large [9]. Specifically, for  $N_{gas} < N_{liq}$  the critical density is shifted to a lower value. The greater the difference between the number of particles in each simulation cell, the larger the shift in the predicted critical density toward a lower value. Even differences between the number of particles in each phase of only 1% were shown to cause substantial shifts in the apparent  $\rho_c^*$ .

The apparent critical pressure is plotted vs  $L^{-(d-1/\nu)}$  in Figure 4.  $p_c^*(L)$  displays the expected linear behavior for the 5 largest system sizes studied when plotted vs  $L^{-(d-1/\nu)}$ . The  $V = 216$  data do not obey our scaling hypothesis, possibly because this system lies outside the region in which the finite-size scaling analysis is valid. Our assumptions about finite-size scaling do not include contributions from irrelevant scaling fields. These fields, while not important for larger system sizes, become significant for smaller systems [18]. In addition, the effects of long-range corrections used in the present work are different for different system sizes and may have an effect on the apparent location of the critical point. Extrapolation to infinite system size yields  $p_c^* = 0.1279(6)$ , which is in reasonable agreement with the value reported by Smit of  $p_c^* = 0.131(1)$  and is consistent with the pressure calculations of [35].

It is interesting to compare our results with the recent study of Caillol [26] on the four-dimensional hypersphere. Caillol determined  $T_c^*(\infty) = 1.326(2)$ ,  $\beta_c \mu_c(\infty) = -2.676(5)$ ,  $\rho_c^*(\infty) = 0.316(2)$  and  $p_c^*(\infty) = 0.147(2)$ . The values for the critical temperature, chemical potential and pressure are not in agreement with our results. System size effects are quite different in the two studies. For example, the change in  $T_c^*$  as a function of system size is

1% over the range  $V = 343$  to  $V = \infty$  in our results, while Caillol's values shift by 7% over a range of  $V = 400$  to  $V = \infty$ . Also, on the four-dimensional hypersphere, smaller system sizes overestimate the critical temperature, while in our study smaller system sizes underestimate the critical temperature, as seen previously by Wilding [18]. For the critical density, both simulation studies give similar results. The largest discrepancies are seen in the critical pressure. While Caillol's results also follow linear behavior when plotted vs  $L^{-(d-1/\nu)}$ , the change in  $p_c^*(L)$  over the range of systems studied is over 80%. In comparison, our results vary by only 4.5% over the range of systems studied.

As an additional check of our methods, we performed a short series of simulations for the Lennard-Jones potential truncated at  $2.5\sigma$ . We calculated  $T_c^* = 1.186(2)$ ,  $\beta_c\mu_c = -2.778(3)$ ,  $\rho_c^* = 0.316(3)$  and  $p_c^* = 0.109(2)$ , which compare favorably with Wilding's previous estimates of  $T_c^* = 1.1876(3)$ ,  $\beta_c\mu_c = -2.778(2)$ ,  $\rho_c^* = 0.3197(4)$  and  $p_c^* = 0.1093(6)$  [18,36].

Since the four-dimensional hypersphere and our system are indistinguishable at the limit of infinite system size, the reasons for the discrepancies between the two sets of estimates are currently unclear. For Caillol's estimates of  $T_c^*$  and  $\rho_c^*$ , the Lennard-Jones equation of state fitted by Johnson *et al* [37] gives  $p_c^* = 0.137$ , a value which is 6.8% lower than his calculated value of  $p_c^* = 0.147(2)$ . At our predicted  $T_c^* = 1.3120(7)$  and  $\rho_c^* = 0.316(1)$ , the equation predicts  $p_c^* = 0.1294$ , a value 1.2% higher than our result of  $p_c^* = 0.1279(6)$ .

## B. Binary Mixture

We now turn our attention to the critical behavior of the binary mixture. As stated earlier, the mixture belongs to the same universality class as the pure fluid. By performing the appropriate mapping of the critical ordering operator distribution to  $\tilde{p}_m^*(x)$  it is possible to calculate the apparent critical parameters. We accomplish the mapping by fixing the temperature, in this case we set  $T^* = 1.0$ , and tuning the field mixing parameters and chemical potentials until the ordering operator distribution collapses onto  $\tilde{p}_m^*(x)$ . Returning to Figure 1, we see that the critical ordering operator distribution for the binary mixture

collapses well onto the universal ordering operator distribution.

The dependence of  $\rho_c^*(L)$  on  $L^{-(d-1/\nu)}$  is shown in Figure 3. Unlike the pure fluid for which  $\rho_c^*(L)$  was nearly invariant with  $L$ , for the mixture there is a clear dependence on system size. This is due to the fact that we see larger field mixing contributions from the energy-like operator in the case of the mixture than in the pure fluid. By performing a linear regression on the simulation data we calculated  $\rho_c^*(\infty) = 0.406(2)$ .

The critical pressure is another quantity of interest. Figure 4 shows the dependence of the apparent critical pressure,  $p_c^*(L)$ , on our proposed scaling variable,  $L^{-(d-1/\nu)}$ . As is the case for the pure fluid, we see a linear dependence of  $p_c^*(L)$  against  $L^{-(d-1/\nu)}$ . This supports our hypothesis that the apparent critical pressure scales with system size in the same way as  $\rho_c^*(L)$  and  $x_{1c}(L)$ . In keeping with our findings for  $\rho_c^*(L)$ , we see a slightly stronger  $L$  dependence on  $p_c^*(L)$  for the mixture than we see for the pure fluid. The change in  $p_c^*(L)$  for the pure fluid over the range of volumes studied was 4.5% while for the mixture it was 5.8%. Again, we attribute this to greater field mixing from the energy-like operator.

In Figure 5 we plot  $x_{1c}(L)$  vs  $L^{-(d-1/\nu)}$ . From the plot we see that the critical solvent mole fraction exhibits a linear dependence. Extrapolation of the data to  $L = \infty$  yields  $x_{1c}(\infty) = 0.459(3)$ .

Finally, we present the results of our study of the subcritical regime. In Figure 6 we plot a pressure-composition phase diagram for  $T^* = 1.0$  and include the data of Harismiadis *et al* [31] for comparison. In addition, the predictions of van der Waals 1 fluid theory with the Lennard-Jones equation of state of Johnson *et al* [37] are included for reference. For clarity, the isotherms  $T^* = 0.90$  and  $T^* = 1.1$  are plotted separately in Figure 7. Selected phase coexistence data for the 3 temperatures studied are listed in Table I. For  $T^* = 1.0$ , our results show considerably less scatter than results previously calculated with the Gibbs ensemble technique. In order to make certain that these reduced uncertainties are not a result of longer runs, we performed a new set of simulations so that a comparison of the statistical uncertainties between histogram reweighting and Gibbs ensemble could be performed on an equal CPU time basis. The results, also shown in 6, show comparable scatter and statistical

uncertainties as the results of Harismiadis *et al.* Therefore, we conclude that for simulations of equal CPU time, the histogram reweighting technique gives data with considerably less scatter and statistical uncertainty than when the Gibbs ensemble is used.

The lower statistical efficiency of the Gibbs ensemble can be traced directly to the volume move. For potentials that do not scale with the length of the simulation cell, a complete recalculation of the energy is necessary, which is an  $O(N^2)$  operation. There is a second, more subtle point, raised by Wilding and Binder with respect to the sampling efficiency of  $NpT$  simulations [36]. They suggested that for a given  $\langle \rho \rangle$  the random walk in  $V$  required to pass from one phase to the other at coexistence was longer than in  $N$ , resulting in a correlation time for the  $NpT$  ensemble that was considerably longer than that of the  $\mu VT$  ensemble. Due to the use of a volume move, one would expect to see a similar increase in correlation time for Gibbs ensemble simulations when compared to simulations in the  $\mu VT$  ensemble.

Over the temperature range studied, the average statistical uncertainties in pressure and liquid and vapor composition were between 0.3 and 0.5%. For these quantities, the statistical uncertainty did not vary much with temperature. The statistical uncertainty in the liquid and vapor densities at the temperature of the simulations ( $T^* = 1.0$ ) was somewhat lower than for the "extrapolated" data at  $T^* = 0.90$  to  $T^* = 1.1$ .

## V. CONCLUSIONS

To summarize, we have applied mixed-field finite-size scaling theory to pure fluids and mixtures interacting with a Lennard-Jones potential. Finite-size effects in our work were considerably smaller than in the study of the full Lennard-Jones potential on a four-dimensional hypersphere [26], but larger than in the case of the truncated Lennard-Jones fluid under periodic boundary conditions [18]. Our analysis leads to the following critical parameters for the pure untruncated Lennard-Jones fluid,  $T_c^* = 1.3120(7)$ ,  $\rho_c^* = 0.316(1)$ ,  $p_c^* = 0.1279(6)$

In addition, we have shown how it is possible to extend the mixed-field finite-size scaling

analysis to mixtures through the addition of a parameter that controls the degree of field mixing from the second component. Greater finite-size effects were seen in the binary mixture when compared to the pure fluid. These effects we attribute to a greater degree of field mixing from the energy-like operator. Despite the larger finite-size effects, a finite-size scaling analysis was still possible and we calculated the following critical parameters for the Lennard-Jones binary mixture with  $\sigma_1 = \sigma_2 = 1.0$  and  $\epsilon_1 = 1.0$ ,  $\epsilon_2 = 0.5$  at  $T^* = 1.0$ ,  $x_{1c} = 0.459(3)$ ,  $\rho_c^* = 0.406(2)$ ,  $p_c^* = 0.1522(9)$

Application of histogram reweighting techniques to mixtures allows for the calculation of pressure-temperature-composition phase diagrams from a small number of simulations. Coexistence data with of much higher quality are obtained relative to Gibbs ensemble calculations of comparable computational time.

## VI. ACKNOWLEDGMENTS

Research on which this manuscript is based was supported the US Department of Energy, Office of Basic Energy Sciences, under grant DEFG02-98ER14C58. We would like to thank Lev Gelb and Nigel Wilding for helpful discussions and Jean-Michel Caillol for providing copies of manuscripts prior to publication. We are grateful to John Valleau for pointing out an error in the original version of the manuscript.

TABLES

TABLE I. Selected phase coexistence data. The numbers in parenthesis indicate the statistical uncertainty in units of the last digit of the corresponding value.

	$p^*$	$x_1$	$y_1$	$\rho_{liq}^*$	$\rho_{gas}^*$
$T^* = 0.90$	0.0136(3)	0.995(1)	0.9115(4)	0.74(1)	0.0162(1)
	0.0154(2)	0.9902(7)	0.8108(2)	0.74(1)	0.0184(1)
	0.0198(2)	0.977(2)	0.6404(8)	0.74(1)	0.0240(2)
	0.03130(7)	0.943(2)	0.424(6)	0.739(3)	0.0399(4)
	0.0618(2)	0.834(3)	0.259(2)	0.711(9)	0.0852(1)
$T^* = 1.0$	0.0284(3)	0.9926(1)	0.9107(3)	0.699(2)	0.0330(1)
	0.0319(3)	0.9835(3)	0.822(1)	0.697(2)	0.0374(2)
	0.0399(2)	0.9628(8)	0.675(3)	0.691(2)	0.0480(6)
	0.05927(6)	0.910(2)	0.500(3)	0.674(2)	0.0749(6)
	0.1064(2)	0.752(6)	0.373(2)	0.610(5)	0.1623(5)
$T^* = 1.1$	0.0521(2)	0.988(3)	0.910(4)	0.63(1)	0.059(1)
	0.0582(3)	0.973(2)	0.828(2)	0.63(1)	0.0659(6)
	0.07166(8)	0.942(2)	0.691(6)	0.626(5)	0.084(2)
	0.1021(3)	0.852(7)	0.571(7)	0.57(2)	0.138(3)

## REFERENCES

- [1] A. Z. Panagiotopoulos, *Mol. Phys.* **61**, 813 (1987).
- [2] A. Z. Panagiotopoulos, N. Quirke, M. Stapleton and D. J. Tildesley, *Mol. Phys.* **63**, 527 (1988).
- [3] B. Smit, Ph. de Smedt, and D. Frenkel, *Mol. Phys.* **68**, 931 (1989).
- [4] F. A. Escobedo and J. J. de Pablo, *J. Chem. Phys.* **103**, 2703 (1995)
- [5] F. A. Escobedo and J. J. de Pablo, *J. Chem. Phys.* **105**, 4391 (1996)
- [6] F. A. Escobedo, *J. Chem. Phys.* **108**, 8761 (1998)
- [7] J. R. Recht and A. Z. Panagiotopoulos, *Mol. Phys.* **80**, 843 (1993).
- [8] A. Z. Panagiotopoulos, *Int. J. Thermophys.* **15**, 1057 (1994).
- [9] J. P. Valleau, *J. Chem. Phys.* **108**, 2962 (1998).
- [10] A. M. Ferrenberg and R. H. Swendsen, *Phys. Rev. Lett.* **61**, 2635 (1988).
- [11] A. M. Ferrenberg and R. H. Swendsen, *Phys. Rev. Lett.* **63**, 1195 (1988).
- [12] R. H. Swendsen, *Physica A* **194**, 53 (1993).
- [13] K. Binder, *Z. Phys. B* **43**, 119 (1981).
- [14] A. M. Ferrenberg and D. P. Landau, *Phys. Rev. B* **44**, 5081 (1991).
- [15] R. B. Griffiths and J. C. Wheeler, *Phys. Rev. A* **2**, 1047 (1970).
- [16] N. B. Wilding and A. D. Bruce, *J. Phys. Condens. Matter* **4**, 3087 (1992).
- [17] A. D. Bruce and N. B. Wilding, *Phys. Rev. Lett.* **68**, 193 (1992).
- [18] N. B. Wilding, *Phys. Rev. E*, **52**, 602 (1995).
- [19] N. B. Wilding and M. Müller, *J. Chem. Phys.* **102**, 2562 (1995).

- [20] A. Z. Panagiotopoulos, V. Wong and M. A. Floriano, *Macromolecules* **31**, 912 (1998).
- [21] E. de Miguel, E. M. del Río and M. M. Telo da Gama, *J. Chem. Phys.* **103**, 6188 (1995).
- [22] N. B. Wilding, F. Schmid, and P. Nielaba *Phys. Rev. E* **58**, 2201 (1998).
- [23] M. Müller and N. B. Wilding, *Phys. Rev. E* **51**, 2079 (1995).
- [24] N. B. Wilding, *Phys. Rev. E* **55**, 6624 (1997).
- [25] B. Smit, *J. Chem. Phys.* **96**, 8639 (1992).
- [26] J. M. Caillol, *J. Chem. Phys.* **109**, 4885 (1998).
- [27] B. A. Berg and T. Neuhaus, *Phys. Rev. Lett.* **68**, 9 (1992).
- [28] J. V. Sengers and J. M. H. Levelt Sengers, *Ann. Rev. Phys. Chem.* **37**, 189 (1986).
- [29] M. A. Anisimov, E. E. Gorodetskii, V. D. Kulikov, and J. V. Sengers, *Phys. Rev. E* **51**, 1199 (1995).
- [30] D. N. Theodorou and U. W. Suter, *J. Chem. Phys.* **82**, 955-965 (1985).
- [31] V. I. Harismiadis, N. K. Koutras, D. P. Tassios and A. Z. Panagiotopoulos, *Fluid Phase Equil.* **65**, 1 (1991).
- [32] A. Lotfi, J. Vrabec and J. Fischer, *Mole. Phys.* **76**, 1319 (1992).
- [33] J. H. Chen, M. E. Fisher and B. G. Nickel, *Phys. Rev. Lett.* **48**, 630 (1982).
- [34] K. K. Mon and K. Binder, *J. Chem. Phys.* **96**, 6989 (1992).
- [35] J. E. Hunter and W. P. Reinhardt, *J. Chem. Phys.* **103**, 8627 (1995).
- [36] N. B. Wilding and K. Binder, *Physica A* **231**, 439 (1996).
- [37] J. K. Johnson, J. A. Zollweg and K. E. Gubbins, *Mol. Phys.* **78**, 591 (1993).

FIGURES

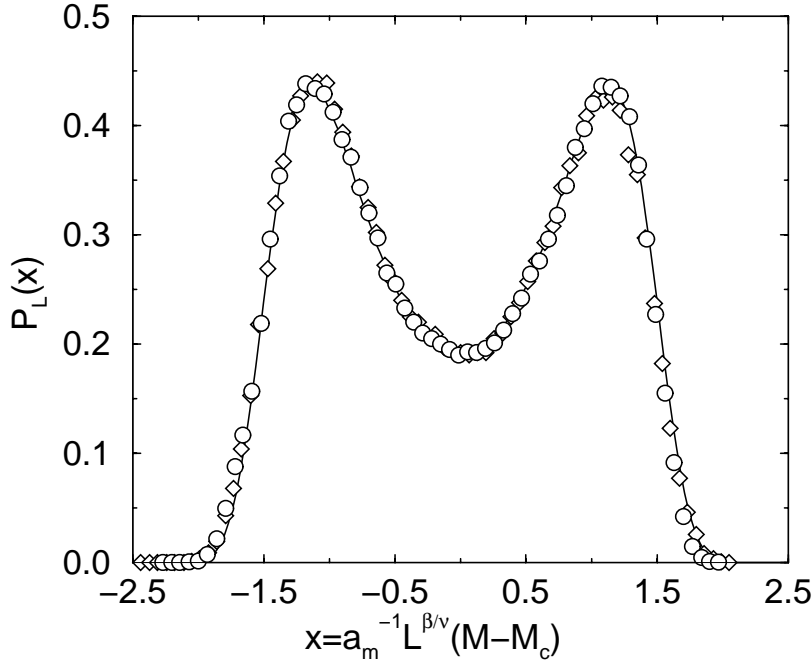


FIG. 1. Ordering operator distribution  $P_L(x)$  for the pure fluid,  $V = 216$  (circles); for the binary mixture at  $T^* = 1.0$ ,  $V = 216$  (diamonds). The solid line represents the universal fixed point ordering operator distribution  $\tilde{P}_m^*(x)$ .

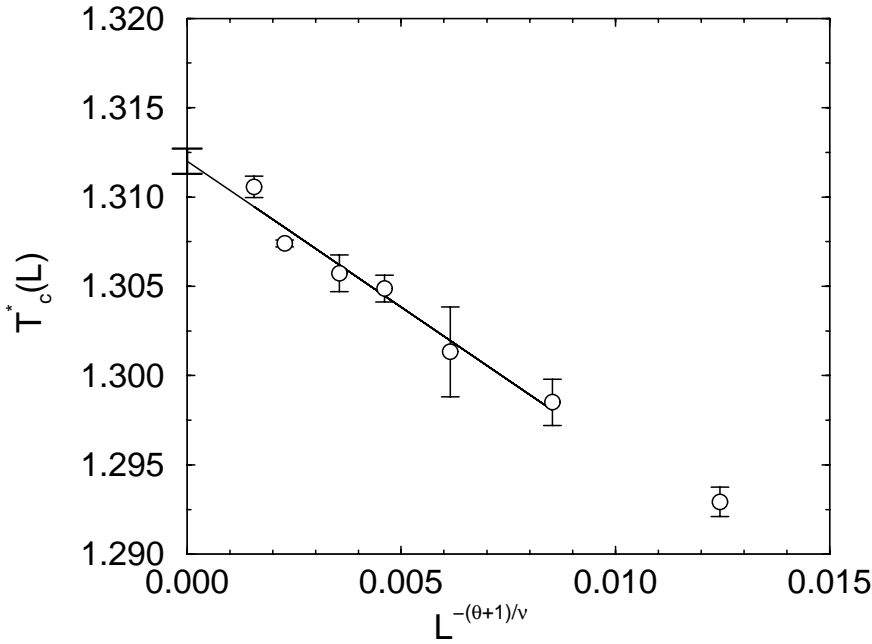


FIG. 2. Apparent critical temperature  $T_c^*(L)$  for the pure Lennard-Jones fluid expressed as a function of  $L^{-(\theta+1)\nu}$ . The line represents least-squares fit of the data.

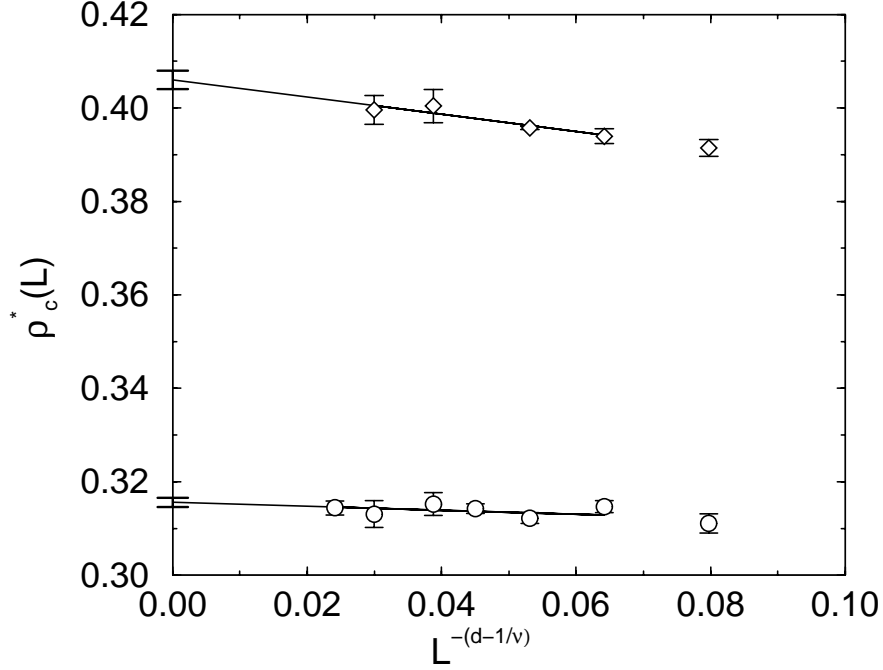


FIG. 3. Apparent critical density  $\rho_c^*(L)$  as a function of  $L^{-(d-1/\nu)}$  for the pure fluid (circles) and the binary mixture (diamonds). The line represents least-squares fit of the data.

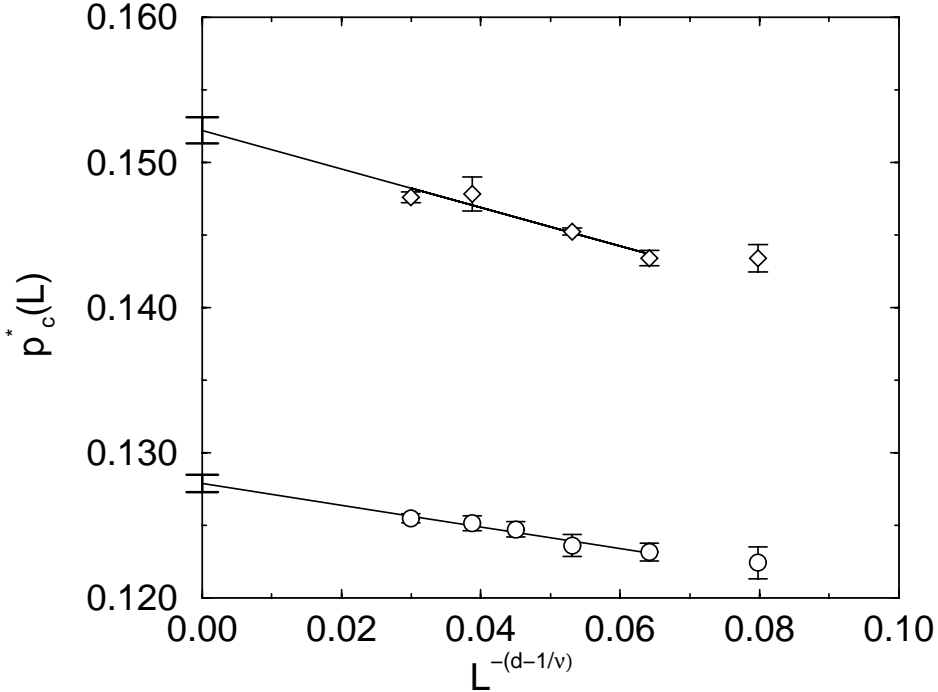


FIG. 4. Apparent critical pressure  $p_c^*(L)$  as a function of  $L^{-(d-1/\nu)}$  for the pure fluid (circles) and the binary mixture (diamonds). The line represents least-squares fit of the data.

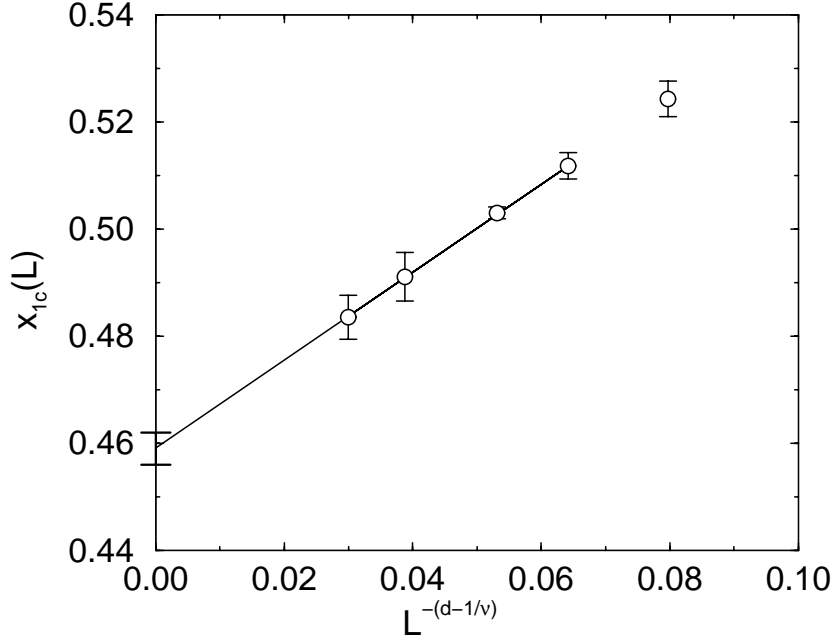


FIG. 5. Apparent critical composition  $x_{1c}(L)$  for the binary Lennard-Jones mixture at  $T^* = 1.0$ , as a function of  $L^{-(d-1/\nu)}$ . The line represents least-squares fit of the data.

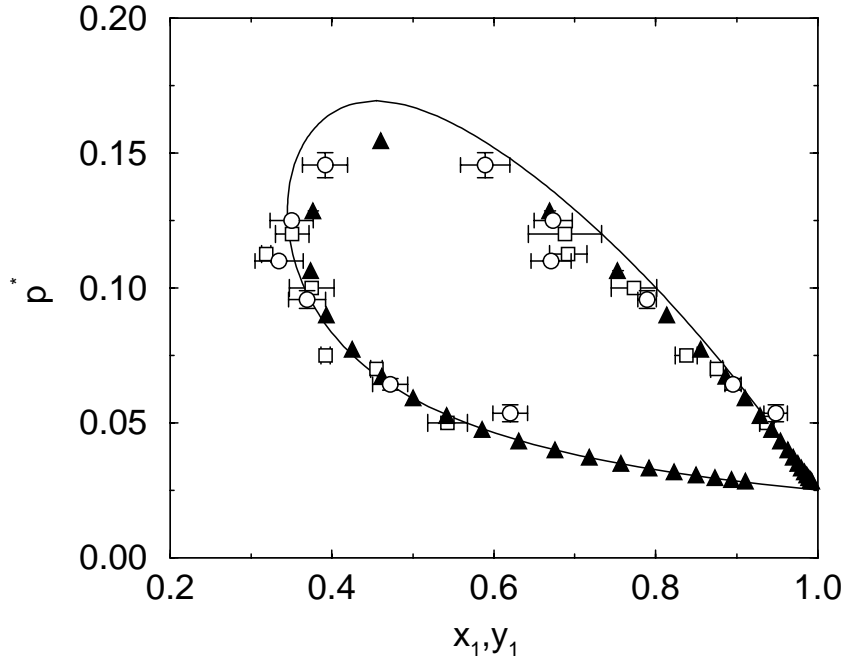


FIG. 6. Pressure-composition diagram for the binary Lennard-Jones mixture with  $\epsilon_1 = 1.0$ ,  $\epsilon_2 = 0.5$ ,  $\sigma_1 = \sigma_2 = 1.0$  at  $T^* = 1.0$ . This work (triangles), Gibbs ensemble (circles) [31], Gibbs ensemble, this work, (squares). Statistical uncertainties for this work are less than the size of the symbols. The solid line represents the predictions of van der Waals 1 fluid theory.

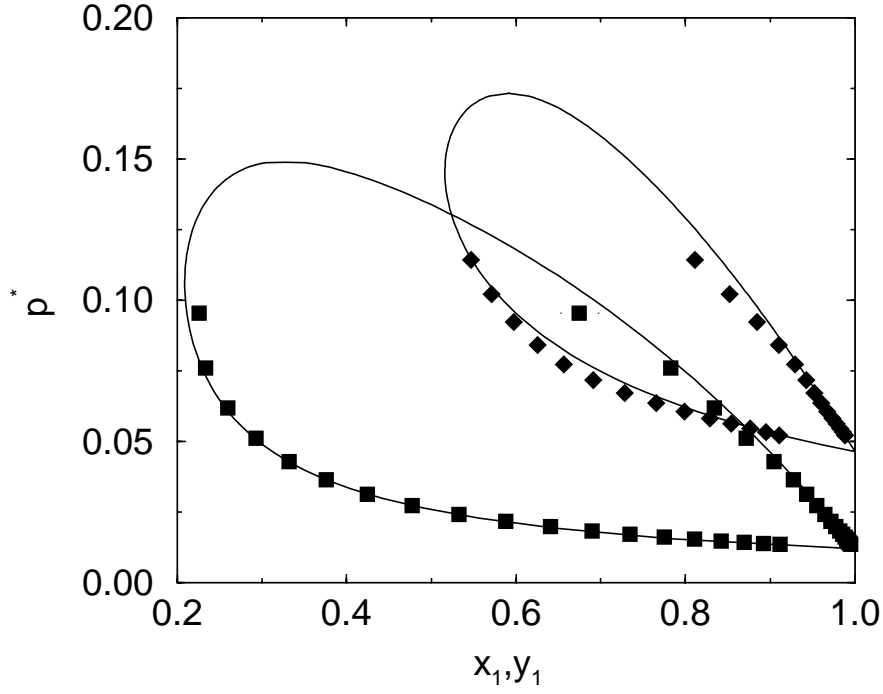


FIG. 7. Additional pressure-composition diagrams for  $\epsilon_1 = 1.0$ ,  $\epsilon_2 = 0.5$ ,  $\sigma_1 = \sigma_2 = 1.0$ .  $T^* = 1.1$  (filled diamonds),  $T^* = 0.90$  (filled squares). Statistical uncertainties are less than the size of the symbols. The line represents the predictions of van der Waals 1 fluid theory.